The EMBO Journal (2012) 31, 2350–2364 | © 2012 European Molecular Biology Organization | Some Rights Reserved 0261-4189/12
www.embojournal.org

THE EMBO JOURNAL

EMBO open

Oligomers of the ATPase EHD2 confine caveolae to the plasma membrane through association with actin

Miriam Stoeber[1], Ina Karen Stoeck[1], Christine Hänni[1], Christopher Karl Ernst Bleck[2], Giuseppe Balistreri[1] and Ari Helenius[1,*]

[1]Institute of Biochemistry, ETH Zurich, Zurich, Switzerland and [2]Center for Cellular Imaging and NanoAnalytics (C-CINA), Biozentrum, University of Basel, Basel, Switzerland

Caveolae are specialized domains present in the plasma membrane (PM) of most mammalian cell types. They function in signalling, membrane regulation, and endocytosis. We found that the Eps-15 homology domain-containing protein 2 (EHD2, an ATPase) associated with the static population of PM caveolae. Recruitment to the PM involved ATP binding, interaction with anionic lipids, and oligomerization into large complexes (60–75S) via interaction of the EH domains with intrinsic NPF/KPF motifs. Hydrolysis of ATP was essential for binding of EHD2 complexes to caveolae. EHD2 was found to undergo dynamic exchange at caveolae, a process that depended on a functional ATPase cycle. Depletion of EHD2 by siRNA or expression of a dominant-negative mutant dramatically increased the fraction of mobile caveolar vesicles coming from the PM. Overexpression of EHD2, in turn, caused confinement of cholera toxin B in caveolae. The confining role of EHD2 relied on its capacity to link caveolae to actin filaments. Thus, EHD2 likely plays a key role in adjusting the balance between PM functions of stationary caveolae and the role of caveolae as vesicular carriers.

The EMBO Journal (2012) **31,** 2350–2364. doi:10.1038/emboj.2012.98; Published online 13 April 2012
Subject Categories: membranes & transport; cell & tissue architecture
Keywords: actin cytoskeleton; ATPase; caveolae; EHD2; endocytosis

Introduction

Caveolae are invaginations in the plasma membrane (PM) with a lipid composition enriched in cholesterol and sphingolipids and two major protein components, the caveolins and the cavins. Caveolins are integral membrane proteins stably associated with each other and cholesterol to form a protein-lipid scaffold that provides the organizing principle of caveolae (Sargiacomo *et al*, 1995; Parton and Simons, 2007; Hayer *et al*, 2010a). Cavins form soluble complexes in the cytosol that bind to the caveolin scaffolds in the PM, and by providing an additional peripheral protein layer they stabilize caveolae and define their morphology (Hill *et al*, 2008; Hansen *et al*, 2009; McMahon *et al*, 2009; Hansen and Nichols, 2010).

Most of the caveolae are immobile and serve as signalling platforms and membrane reservoirs in the PM (Parton and Simons, 2007; Sinha *et al*, 2011). Several studies have suggested that they are associated with actin microfilaments (Rothberg *et al*, 1992; Stahlhut and van Deurs, 2000; Richter *et al*, 2008). Interactions between components of the cytoskeleton and caveolae are likely to control dynamics of caveolae (Stahlhut and van Deurs, 2000; Mundy *et al*, 2002; Foti *et al*, 2007; Sverdlov *et al*, 2009). Caveolae can be activated through external or internal stimuli to undergo internalization and to carry cargo from the PM to early endosomes (EEs) (Parton *et al*, 1994; Thomsen *et al*, 2002; Botos *et al*, 2008; Lajoie and Nabi, 2010). The endocytic process requires dynamin, local actin rearrangements, and phosphorylation events (Oh *et al*, 1998; Mundy *et al*, 2002; Pelkmans and Helenius, 2002; Pelkmans *et al*, 2005; Sverdlov *et al*, 2007). It is not clear which cellular factors regulate the balance between static caveolae and motile caveolar carriers.

In this paper, we focus on Eps-15 homology domain-containing protein 2 (EHD2), an ATPase that binds to the PM. In a proteomics study, Aboulaich *et al* (2004) detected EHD2 as one of the numerous proteins present in preparations of caveolae isolated from human adipocytes. More recently, Hansen *et al* (2011) expressed EHD2 as a fluorescent fusion protein in HeLa cells and found that it colocalized with CAV1.

While EHD2 is structurally well characterized, the cellular functions remain elusive. It belongs to a dynamin-related family of proteins of which the three others members (EHD1, 3, and 4) are involved in the regulation of endocytic transport at the level of the endosomal recycling compartment (Naslavsky and Caplan, 2011). These three play a role in receptor sorting and recycling (Blume *et al*, 2007; George *et al*, 2007; Sharma *et al*, 2008). EHD2 shares its overall domain structure with the other EHDs (Figure 1A), and has a central G domain, which binds and slowly hydrolyses ATP (Lee *et al*, 2005; Daumke *et al*, 2007). It associates with the PM, forms homooligomers instead of heterooligomers (George *et al*, 2007), and tubulates liposomes *in vitro* by forming oligomers around them (Daumke *et al*, 2007). The crystal structure of the EHD2 dimer shows the two G domains with flanking helical domains organized into a compact scissor-shape structure with a curved surface as the site of interaction with lipids (Figure 1A; Daumke *et al*, 2007). EH domains are located on top of the G domains. They are proposed to mediate homooligomerization by binding to intrinsic NPF motifs in adjacent EHD2 dimers (Daumke *et al*, 2007).

We address the assembly and functions of EHD2 using biochemistry- and microscopy-based approaches. Our results show a progressive series of events that lead to the formation of EHD2 complexes, and the association of these complexes

*Corresponding author. Institute of Biochemistry, ETH Zurich, Schafmattstrasse 18, Zurich CH-8093, Switzerland.
Tel.: +41 44 632 68 17; Fax: +41 44 632 12 69;
E-mail: ari.helenius@bc.biol.ethz.ch

Received: 24 February 2012; accepted: 23 March 2012; published online: 13 April 2012

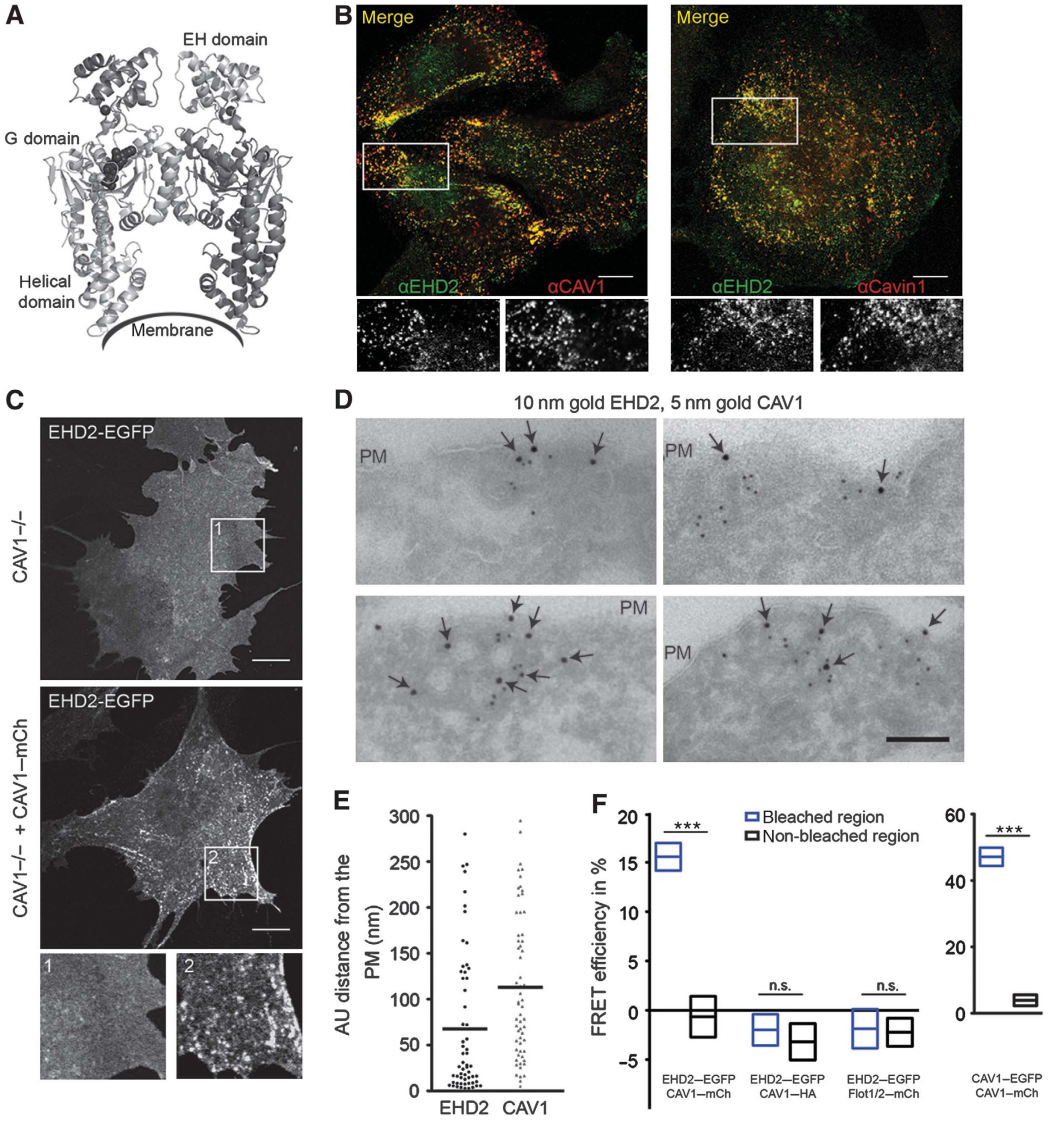

Figure 1 EHD2 is associated with plasma membrane caveolae. (**A**) Scissor-shape structure of the EHD2 dimer. The membrane interaction site and domains of one EHD2 molecule are depicted (pdb entry 2QPD) (Daumke et al, 2007). (**B**) Confocal images of HeLa cells stained with anti-EHD2 and anti-CAV1 or anti-EHD2 and anti-cavin-1 antibodies. Lower row shows enlargement of indicated regions in the merged images. Scale bars 10 μm. (**C**) Confocal image of MEF CAV1 −/− cells transfected with EHD2–EGFP only or EHD2–EGFP and CAV1–mCherry for 6 h. Enlargement of indicated regions is shown. Scale bars 10 μm. (**D**) Gallery of electron micrographs of CV1 cells expressing EHD2–EGFP and CAV1–HA for 6 h. Cells were fixed, cryo-sectioned, and immunolabelled with anti-GFP (10 nm gold, arrows) and anti-HA (5 nm gold). Scale bar 100 nm. (**E**) Distance of EHD2- and CAV1-gold particles from the PM in EM micrographs. Scatter dot plot shows 60 perpendicular measurements towards the PM with a maximal distance of 300 nm. Bars represent mean of distributions. (**F**) FRET efficiencies in bleached and non-bleached regions of fixed CV1 cells expressing the indicated plasmids using confocal microscopy and acceptor photobleaching. Graphs show mean FRET efficiencies with 95% confidence intervals. $n = 19$, 8, 9, and 10 cells for EHD2–EGFP/CAV1–mCherry, EHD2–EGFP/CAV1–HA, EHD2–EGFP/Flot1,2–mCherry, and CAV1–EGFP/CAV1–mCherry, respectively. Significance of mean differences between bleached and non-bleached regions was calculated with a two-tailed paired *t*-test. ***P-value < 0.0001, n.s.: not significant.

with caveolae in the PM. The EHD2 plays an important role in regulating caveolar dynamics. Our data provide evidence that EHD2 confines caveolae to the PM by providing a link to actin filaments.

Results

EHD2 is associated with caveolae

When fluorescent EHD2 (EHD2–EGFP) and caveolin-1 (CAV1–mCherry) were co-expressed in CV1 or HeLa cells, they colocalized within numerous small puncta in the PM (Supplementary Figure S1A). Total-internal reflection fluorescent microscopy (TIR-FM) allowed us to determine that 95% of CAV1–mCherry-positive spots in the PM contained EHD2–EGFP (Supplementary Figure S1B). Fluorescent versions of cavin-1 and cavin-2 also colocalized with EHD2–EGFP in spots, indicating that the spots were caveolae. The EHD2 signal did not overlap with puncta containing fluorescent clathrin light chain or flotillin1/2 (Supplementary Figure S1C and D). Moreover, using indirect immunofluorescence, we found that endogenous EHD2 was also enriched in cell surface spots positive for endogenous CAV1 and cavin-1 in HeLa, 3T3L1, and A549 cells (Figure 1B; Supplementary Figure S2A). For the endogenous EHD2, we observed in

addition diffuse staining in the cytosol and nucleus showing that there was a pool of free EHD2.

In mouse embryonic fibroblasts (MEFs) devoid of CAV1 (CAV1 −/−), ectopically expressed EHD2 was diffusely distributed in the cytosol and PM. Expression of CAV1 in such cells has been shown to drive caveolae formation (Fra *et al*, 1995). When CAV1 was expressed in the CAV −/− MEFs, we rescued the localization of EHD2 in PM spots (Figure 1C). This indicated that the presence of CAV1 was sufficient to induce efficient accumulation of EHD2 in PM puncta.

To visualize the distribution of EHD2 and CAV1 by electron microscopy (EM), we immunogold labelled cryo-sections from CV1 cells expressing EHD2–EGFP and CAV1–HA with anti-GFP and anti-HA antibodies and 10 or 5 nm gold particles, respectively. Invaginated caveolar structures in the PM were observed and many of them were positive for both CAV1 and EHD2 (Figure 1D). Of the EHD2 gold particles in proximity to CAV1, 92% were localized at invaginated caveolae and caveolar clusters. In contrast to CAV1, gold-labelled EHD2 was not evenly distributed over the entire caveolar invagination but rather localized closer to the rim as quantified in Figure 1E.

We concluded that EHD2 associated with the majority of caveolae in the PM. The association involved indented caveolae and caveolar clusters. When the cellular localization of the three other EHD family members was analysed by confocal microscopy, fluorescent forms of EHD1 and EHD3 were not detected in caveolae but in vesicular and tubular structures. EHD4, the closest homologue of EHD2, was present in 10% of CAV1-positive spots (Supplementary Figure S2B).

EHD2 molecules are in close proximity to CAV1

Immunoprecipitation with antibodies against CAV1 and cavin-1 failed to bring down detectable amounts of EHD2 and *vice versa*, suggesting that EHD2 molecules did not interact strongly with these caveolar proteins (not shown). To examine whether EHD2 was in close proximity to CAV1, fluorescence resonance energy transfer (FRET) was measured. We analysed the effect of acceptor (X-mCherry) photobleaching on the fluorescence intensity of donor (Y-EGFP) molecules in fixed CV1 cells (see Materials and methods). FRET efficiencies were quantified in individual PM puncta within bleached versus non-bleached regions of cells (Figure 1F).

The average FRET efficiency between EHD2–EGFP and CAV1–mCherry in puncta located in bleached regions was 16%. This was significantly higher than in non-bleached regions (Figure 1F). No difference in FRET efficiencies of bleached versus non-bleached regions was detected when EHD2–EGFP was co-expressed with flotillin1/2–mCherry or in our negative control (EHD2–EGFP, CAV1–HA). In cells co-expressing CAV1–EGFP and CAV1–mCherry, the measured FRET efficiency was 48%, i.e., consistent with tightly knit CAV1 homooligomers (Figure 1F; Sargiacomo *et al*, 1995). Thus, EHD2 and CAV1 molecules in caveolae were close to each other but probably not interacting directly.

EHD2 regulates caveolar motility

What could be the functional role of EHD2 associated with caveolae? To address this question, we used RNA interference to deplete cellular EHD2 in HeLa cells. After depletion of over 90% of EHD2 (Figure 2A), CAV1 was still detectable in spots and the oligomeric state of CAV1 was not altered as determined by sucrose velocity gradient centrifugation (Supplementary Figure S3A and B). Both assays had been used earlier to reveal the role of cavin-1 in the maintenance of stable caveolar domains (Hayer *et al*, 2010b). Thus, EHD2 did not seem to be required for caveolar formation and stability.

Strikingly, when live cells stably expressing CAV1–EGFP at low levels were imaged (Supplementary Figure S3C), a dramatic change in caveolar dynamics was observed after EHD2 depletion (Supplementary Movie S1). A significantly greater number of CAV1 spots were now moving rapidly through the cytoplasm in all directions. To quantify the increase in motility, we bleached CAV1–EGFP in a peripheral region of the cell and measured fluorescence recovery over time by confocal microscopy (see Materials and methods; Supplementary Movies S2 and S3). In cells transfected with non-targeting control siRNAs, recovery of signal in the bleached volume was slow in agreement with previous studies on caveolar motility (Thomsen *et al*, 2002; Tagawa *et al*, 2005). This indicated that in our stable cell line, CAV1–EGFP spots represented assembled caveolae. After 12 min, 34% of the initial intensity had recovered (Figure 2B).

After depletion of EHD2, we measured a significantly increased recovery of 75 and 70% of CAV1–EGFP signal using two different siRNA oligonucleotides (Figure 2B and C; Supplementary Movie S3). When EHD2–mCherry was expressed in EHD2-depleted cells, the original phenotype with mainly stationary caveolae could be rescued and CAV1–EGFP recovered only to 27% (Figure 2C).

Next, we studied the effect of EHD2 depletion on the motility of cavin-1, which binds to caveolar domains after these have arrived at the PM form the Golgi complex (Hill *et al*, 2008; Hayer *et al*, 2010a). Cavin-1 does not bind to unassembled CAV1 or to CAV1 in passage through the secretory pathway (Hill *et al*, 2008). However, cavin-1 can be detected in mobile caveolar vesicles (Boucrot *et al*, 2011), and it follows CAV1 from the PM to EEs (Hayer *et al*, 2010b). In a cell line stably expressing cavin-1–EGFP (Supplementary Figure S3C), we detected significantly more movement of cavin-1–EGFP vesicles after EHD2 silencing than in control cells treated with non-targeting siRNA (Figure 2D). As the motility of both CAV1 and cavin-1 was significantly increased, we concluded that the mobile vesicles were most likely derived from the PM.

Budding of caveolae from the PM requires dynamin (Henley *et al*, 1998; Oh *et al*, 1998). We expressed the dominant-negative dynamin-K44A mutant in cells treated with EHD2 siRNA. Strikingly, the extent of CAV1 movement was now significantly decreased in comparison with control cells (Figure 2E). This was consistent with the mobile caveolar vesicles being derived from the PM and with a role of EHD2 in restraining caveolae to the PM.

EHD2-positive caveolae confine cholera toxin to the PM

The uptake of cholera toxin (CT) into mammalian cells can be mediated by several endocytic mechanisms (Kirkham *et al*, 2005; Chinnapen *et al*, 2007). The role of caveolae has been intensively studied as they are enriched in the ganglisode GM1, to which the B subunits of CT (CT-B) bind (Parton, 1994; Chinnapen *et al*, 2007). We investigated the

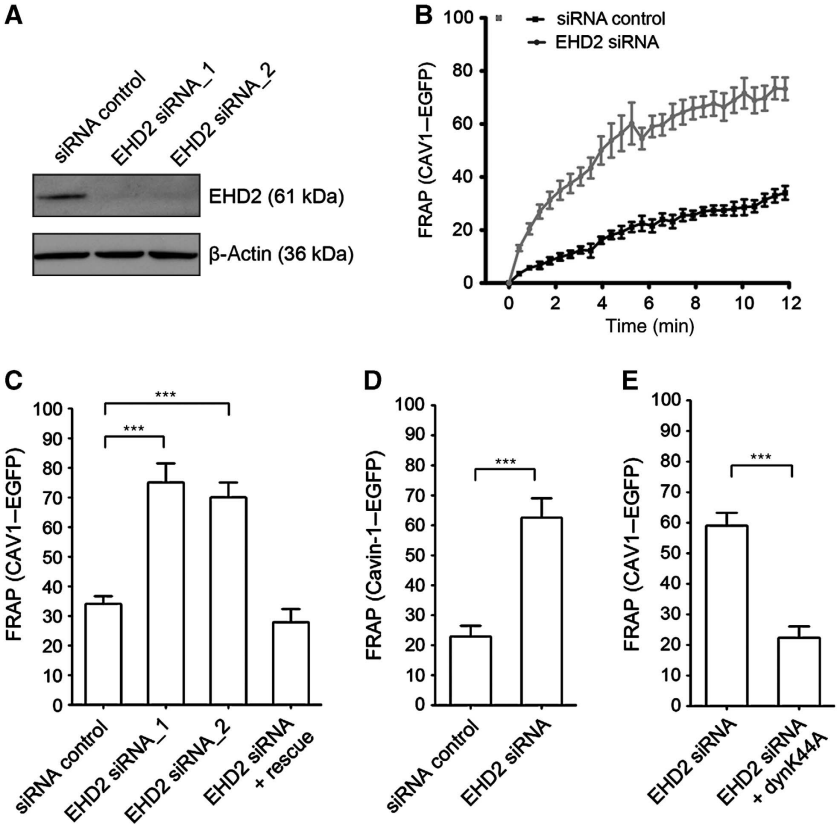

Figure 2 EHD2 regulates motility of caveolae. (**A**) HeLa cells were transfected with siRNA targeting EHD2 or non-targeting siRNA (siRNA control) and cell lysates were analysed after 72 h by SDS–PAGE/western blot using the indicated antibodies. (**B**) Large regions in the cell periphery of HeLa cells, stably expressing CAV1–EGFP, were bleached and the movement of CAV1–EGFP back into the bleached region monitored through fluorescence recovery. Intensities before and directly after bleaching ($t=0$) were normalized to 100 and 0%. Cells were imaged every 20 s for 12 min. Recovery curves for cells treated with siRNA control ($n=12$) or EHD2 siRNA ($n=19$) are presented. Data points present mean values ± s.e.m. (**C**) Relative CAV1 fluorescence 12 min after bleaching in cells transfected with siRNA control ($n=12$), EHD2 siRNA oligo1 ($n=12$) or oligo2 ($n=7$) or after EHD2 silencing and transfection with EHD2–mCherry rescue ($n=10$). (**D**) Relative cavin-1–EGFP signal 12 min after bleaching in HeLa cells, stably expressing cavin-1–EGFP, transfected with siRNA control ($n=9$) or EHD2 siRNA ($n=7$). (**E**) Relative CAV1 fluorescence 8 min after bleaching in HeLa cells transfected with EHD2 siRNA ($n=12$) or after EHD2 silencing and transfection with dyn-K44A-RFP ($n=6$). All bars represent mean ± s.e.m. Significance of mean differences between the conditions was analysed with a two-tailed unpaired *t*-test. ***P-values <0.0001.

effect of EHD2 on CT-B uptake in CV1 cells. After incubation of CV1 cells with a very low concentration of fluorescently labelled CT-B for 30 min followed by a 30-min chase (see Materials and methods), the majority of CT-B was found in giantin-positive Golgi structures (Figure 3A). However when EHD2 was overexpressed, there was a significant reduction of CT-B signal in the Golgi area (Figure 3A and B). Now the PM contained many CT-B-positive spots that colocalized with EHD2 (Figure 3C). In time-lapse movies, we found that the observed EHD2- and CT-B-positive spots at the PM were static (not shown). All the puncta were also positive for endogenous CAV1 showing that clustering of CT-B occurred in PM caveolae (Figure 3D).

The localization of CT-B in caveolae even after long incubation periods has been reported previously (van Deurs *et al*, 2003). To test whether EHD2 influenced trapping of CT-B by caveolae, we quantified the percentage of caveolae that colocalized with CT-B in cells overexpressing EHD2 and control cells. Strikingly, nearly 100% of caveolae positive for both endogenous CAV1 and fluorescent EHD2 contained CT-B (Figure 3E). In control cells, only 50% of caveolae were positive for CT-B. We concluded that elevated levels of EHD2 impaired proper trafficking of CT-B to the Golgi apparatus by confining CT-B to stationary caveolae at the PM.

EHD2 is limited to stationary caveolae in the PM where it cycles on and off

In TIR-FM time-lapse movies of CV1 cells expressing CAV1–mCherry and EHD2–EGFP, we could easily distinguish stationary and mobile CAV1 puncta. A merge of both channels revealed nearly 100% overlap of CAV1–mCherry and EHD2–EGFP signal in caveolae that did not move during the 4-min movie (Supplementary Movie S4). In contrast, CAV1 spots that were mobile were not enriched in EHD2 (Figure 4A; Supplementary Movie S4). That EHD2 was only detected in stationary caveolae raised the possibility that, unlike the cavins, EHD2 proteins were removed during or shortly after caveolae detachment from the PM.

We have previously shown that caveolar domains are not only present in the PM but also associated with EEs where they contain cavin-1 (Pelkmans *et al*, 2004; Hayer *et al*, 2010b). When we transiently overexpressed CAV1–HA to enhance CAV1 trafficking to EE (Hayer *et al*, 2010b), we could readily detect endogenous cavin-1 in Rab5-positive

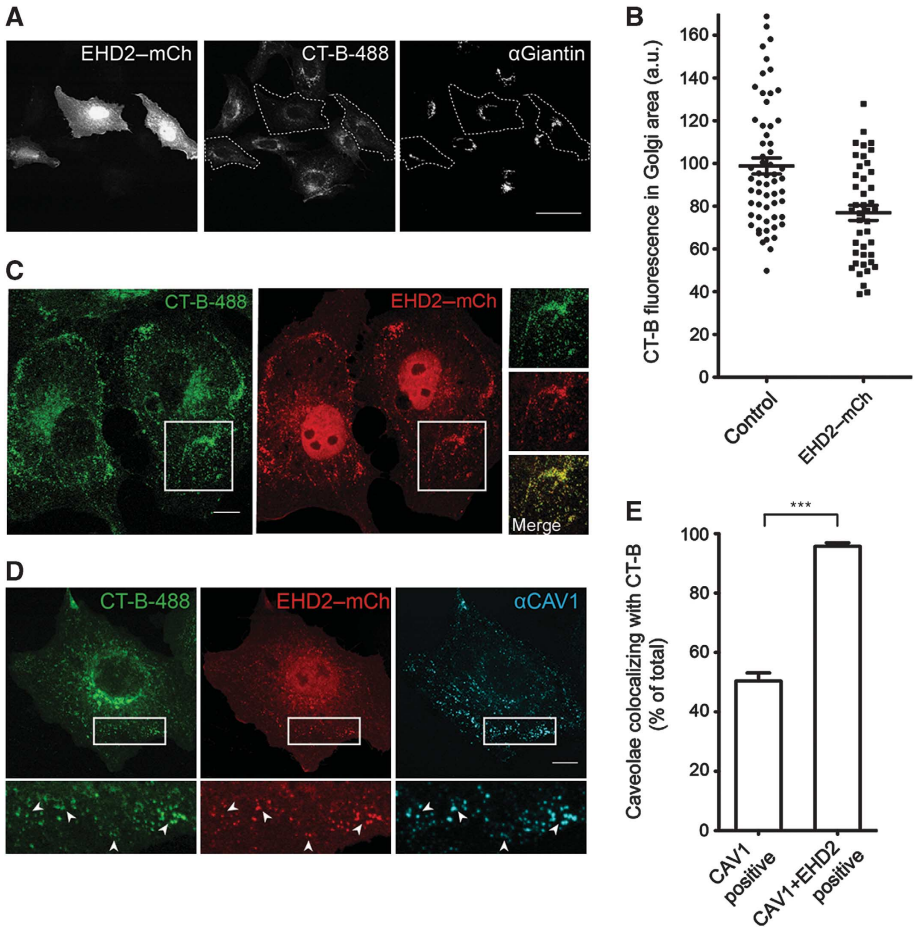

Figure 3 EHD2-positive caveolae confine cholera toxin B to the plasma membrane. (**A**) CV1 cells expressing EHD2–mCherry were incubated with fluorescent CT-B-488 for 30 min and chased for 30 min. Cells were immunostained with anti-Giantin antibodies and analysed by confocal microscopy; the focus was set to the Golgi apparatus. Marked cells express EHD2–mCherry and show decreased CT-B signal in Golgi area. Scale bar 50 μm. (**B**) Quantification of the mean CT-B-488 fluorescence in the Golgi region defined by anti-Giantin staining of non-transfected control cells and EHD2–mCherry-transfected cells. Scatter dot plots show all data points and the mean ± s.e.m. (**C**) CV1 cells expressing EHD2–mCherry were incubated with CT-B-488 as in (**A**). Confocal image with the focus on the plasma membrane is shown; the insets highlight colocalization of CT-B and EHD2 in puncta. Scale bar 10 μm. (**D**) Cells (as in **B**) were stained for endogenous CAV1. Arrows in the magnification highlight colocalization of CT-B, EHD2, and CAV1. Scale bar 10 μm. (**E**) Quantification of caveolae colocalizing with CT-B after 30 min incubation and 30 min chase (as in **A**). Cells were stained for endogenous CAV1 and imaged with focus on the plasma membrane by confocal microscopy. In non-transfected cells, CAV1-positive spots were analysed. In EHD2-transfected cells, CAV1 and EHD2–mCherry-positive spots were analysed. Ten cells were analysed for each condition. Bars represent mean ± s.e.m. Significance was analysed with a two-tailed unpaired *t*-test. ***P-value < 0.0001.

EE (Supplementary Figure S3D). While EHD2 and CAV1 colocalized in PM spots, we did not observe endogenous EHD2 associated with endosomes (Figure 4B). Thus unlike cavin proteins, EHD2 did not traffic with caveolae to EE.

To investigate the dynamics of EHD2 binding to PM caveolae, we used fluorescence recovery after photobleaching (FRAP) and compared recovery rates of bleached, EGFP-tagged EHD2, cavin-1, cavin-2 at static caveolae (Figure 4C–E). Cavin-1 and cavin-2 recovered slowly (<20% in 12 min), and did not reappear in caveolar puncta. This showed that cavin-1 and cavin-2 in caveolae did not exchange with the free pool consistent with previous suggestions (Hill *et al*, 2008; Hayer *et al*, 2010a). In contrast, EHD2–EGFP recovered to 80% of the initial signal intensity in the photobleached area during the 12-min acquisition time (Figure 4D and E). Caveolar EHD2 underwent dynamic exchange with a half-life of 2–4 min. Since the EHD2 signal reappeared precisely in the initially bleached spots positive for CAV1, the turnover occurred at stationary caveolae (Figure 4E). We concluded that EHD2–EGFP molecules associated with static caveolae underwent continuous cycles of association and dissociation.

Multiple domains are required for targeting EHD2 to caveolae

To gain insights into the mode of association with caveolae, we determined the cellular distribution of a panel of EHD2 mutants after expression in CV1 cells (Figure 5A). EGFP fusions of the mutant proteins were transiently expressed in cells for 6–8 h and endogenous CAV1 was stained. Representative confocal microscopy images with the focus on the PM are shown in Figure 5B.

A point mutation in the lipid-binding motif (K327D) was found to block association with caveolae; the mutant protein localized to the cytosol and the nucleus. Mutations in the KPF and NPF motif (KPF/NPF) and deletion of the EH domain

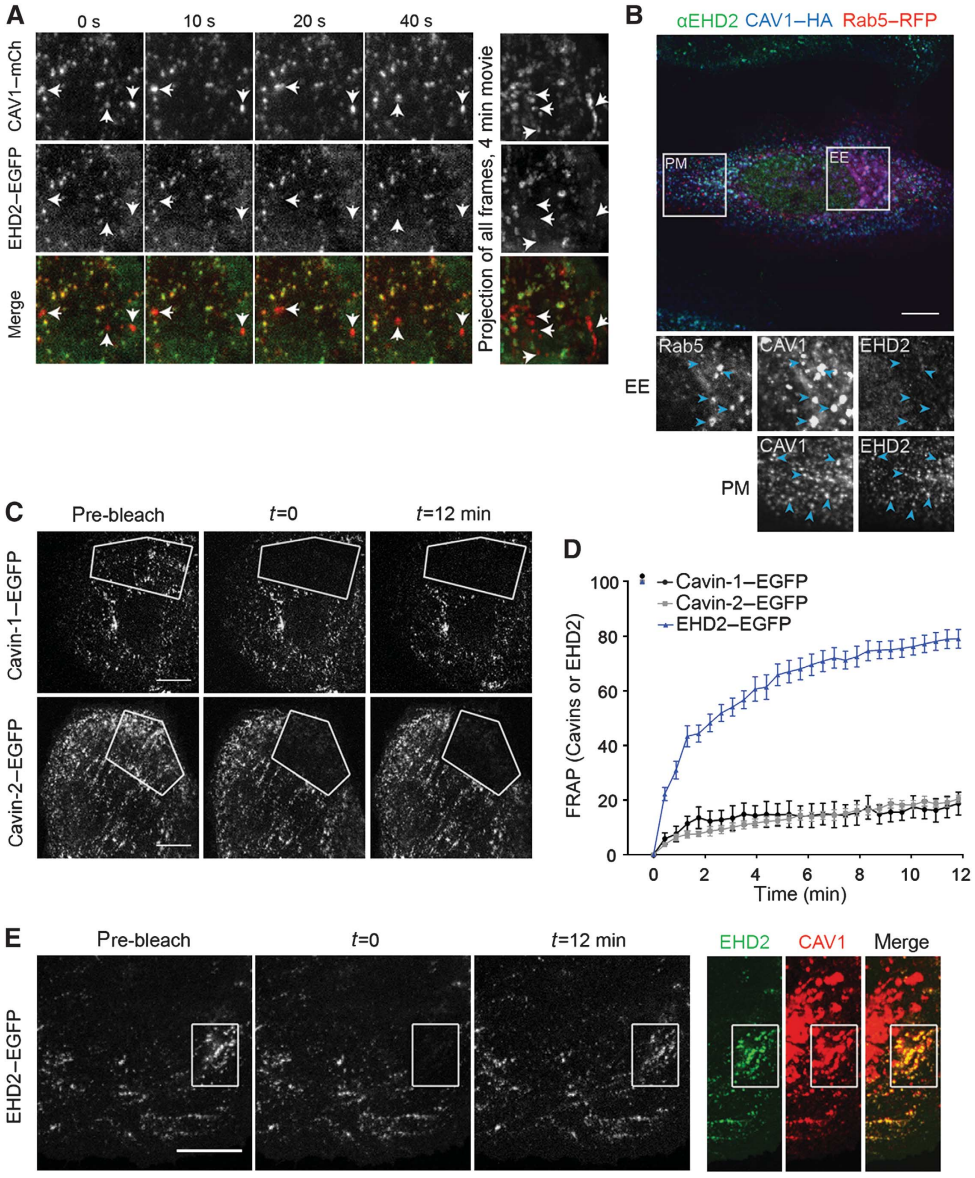

Figure 4 EHD2 is limited to stationary caveolae in the plasma membrane and undergoes dynamic exchange. (**A**) TIRF images (10 s intervals) of a time-lapse series of a CV1 cell, co-expressing EHD2–EGFP and CAV1–mCherry. Right panel: Maximum intensity projection of all frames of the 4-min movie with a frame rate of 0.5 Hz. Arrows highlight moving caveolae devoid of EHD2. Scale bar 10 μm. (**B**) Confocal image of a HeLa cell expressing CAV1–HA and Rab5-RFP for 16 h, immunostained for CAV1 and endogenous EHD2. Highlighted areas are enlarged and show EE or PM regions. Arrows point to EE or PM spots. (**C**) Representative confocal images of FRAP experiments with cavin-1–EGFP or cavin-2–EGFP expressing cells. No fluorescence recovery can be detected during the recorded time. Scale bars 10 μm. (**D**) FRAP curves of transfected CV1 cells. Relative EGFP intensity of indicated fusion proteins in bleached regions. Intensities before and directly after bleaching ($t = 0$) were set to 100 and 0%, respectively. Images were recorded every 20 s for 12 min. $n = 10$, 9, and 6 for EHD2–EGFP, cavin-1–EGFP, and cavin-2–EGFP, respectively. (**E**) Representative confocal images of FRAP experiments with EHD2–EGFP expressing cells. EHD2–EGFP signal reappears at initially bleached spots. Right panels: Spots are positive for co-expressed CAV1–mCherry. Scale bar 10 μm.

(ΔEH) also abolished colocalization of EHD2 with CAV1; EHD2 was diffusely distributed over the PM.

In previous *in-vitro* assays, three G domain mutants were shown to be defective or altered in their interactions with ATP: EHD2-T72A was deficient in ATP binding, EHD2-T94A in ATPase activity, and EHD2-I157Q exhibited a significantly elevated ATP hydrolysis rate (Daumke *et al*, 2007). When expressed in CV1 cells, neither EHD2-T72A nor EHD2-T94A localized to caveolae. They had a diffuse cytosolic and/or membrane-associated distribution. EHD2-I157Q, however, showed a striking punctate distribution colocalizing with endogenous CAV1 in the PM (Figure 5B).

After prolonged expression of all EHD2 mutant constructs (>16 h), we frequently observed the formation of filopodia in agreement with previous reports (Guilherme *et al*, 2004) and found accumulation of EHD2 in the nucleus.

While the EHD2 mutants that did not colocalize with caveolae did not affect CAV1 distribution in fixed cells, we noticed that expression of EHD2-I157Q or wild-type EHD2 for >16 h altered the appearance of the immunostained CAV1. The signal intensity of CAV1 per diffraction-limited caveolar spot was significantly increased in the EHD2 overexpressing cells (Supplementary Figure S4A–C). Given that individual caveolae contain a defined number of CAV1 molecules

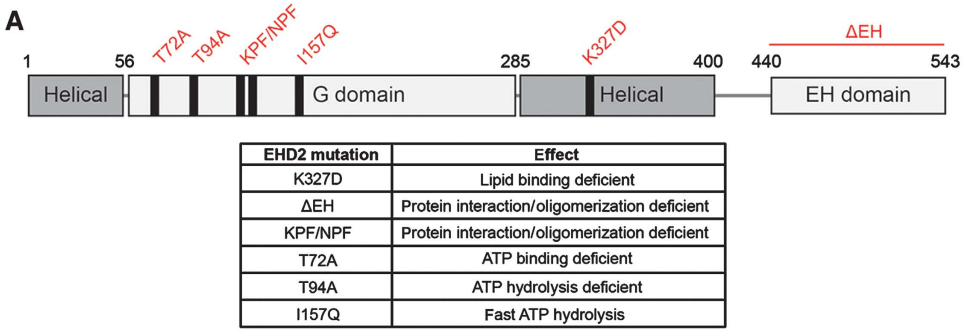

EHD2 mutation	Effect
K327D	Lipid binding deficient
ΔEH	Protein interaction/oligomerization deficient
KPF/NPF	Protein interaction/oligomerization deficient
T72A	ATP binding deficient
T94A	ATP hydrolysis deficient
I157Q	Fast ATP hydrolysis

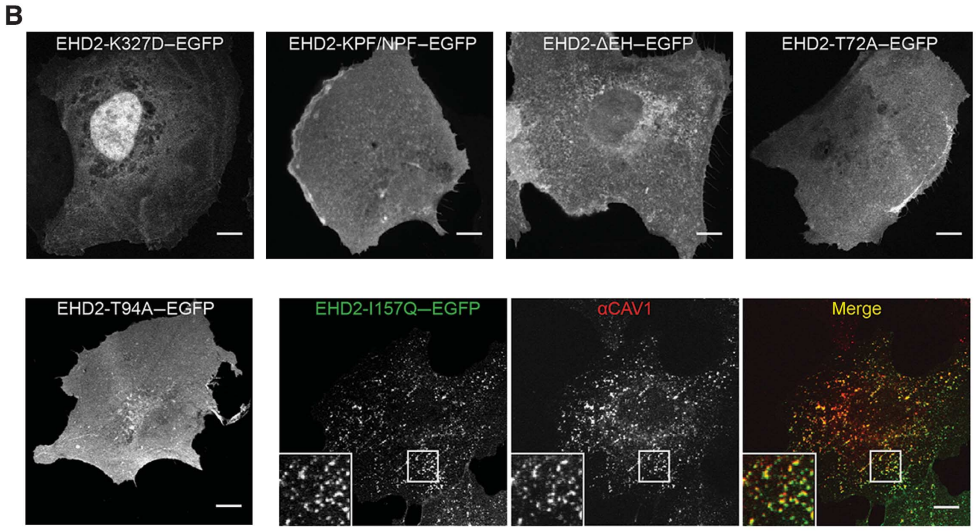

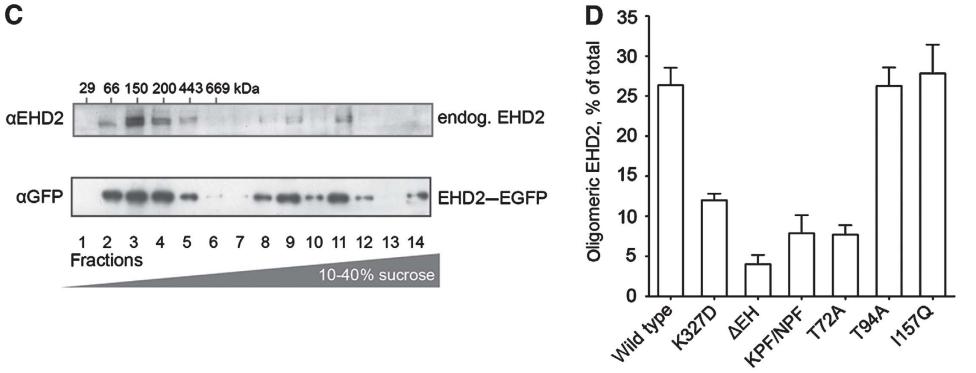

Figure 5 Mutations in EHD2 impair association with caveolae and formation of large EHD2 complexes. (**A**) Domain structure of EHD2 with generated point and deletion mutants and table summarizing effects of these mutations described in previous studies (Guilherme *et al*, 2004; Daumke *et al*, 2007). (**B**) Confocal images of CV1 cells transiently expressing EGFP fusions of EHD2 mutants for 6–8 h. Cells were fixed and stained for endogenous CAV1 (only shown for EHD2-I157Q–EGFP as the other mutants did not colocalize with CAV1). Scale bar 10 μm. (**C**) Cell lysates prepared from 3T3-L1 cells or HeLa cells expressing EHD2–EGFP were run through 10–40% sucrose velocity gradients and fractions analysed by SDS–PAGE/western blot. In both cell lysates, EHD2 was present in distinct oligomeric species sedimenting at 8S, 60S, and 75S (Hayer *et al*, 2010a). 3T3-L1 fractions were analysed with anti-EHD2 antibodies and HeLa fractions with anti-GFP antibodies. (**D**) EHD2 mutants were analysed for their ability to form protein complexes with sedimentation coefficients >60S. EGFP fusions of mutant proteins were expressed for 6–12 h in HeLa cells and lysates run through sucrose velocity gradients (as in **C**). Fractions were analysed with anti-EHD2 antibodies. Bars present mean ± s.e.m. of relative EHD2 signal in fractions 9–12 ('oligomeric EHD2') from three independent experiments.

(Pelkmans and Zerial, 2005; Tagawa *et al*, 2005) and with the assumption that EHD2 association does not alter the accessibility of CAV1 epitopes, our results indicated that elevated cellular levels of wild-type EHD2 and EHD2-I157Q enhanced the formation of clusters of multiple caveolae.

Taken together, the results showed that several domains in EHD2 were required for targeting the protein to the PM and to caveolae; the lipid-binding residues that allow association with negatively charged phospholipids (Daumke *et al*, 2007), the protein interaction and/or oligomerization domains, and the ATPase-containing G domain. A functional ATP binding and hydrolysis cycle was apparently essential for enrichment in caveolae.

Association with caveolae requires EHD2 oligomerization

Based on the topology of domains revealed by the crystal structure and *in-vitro* assays, it has been proposed that EHD2

dimers form oligomers when associated with membranes (Daumke *et al*, 2007). To analyse the oligomeric state of EHD2 proteins in cells, we prepared HeLa and 3T3L1 cell lysates with Triton X-100 and subjected them to sucrose velocity gradient centrifugation (Figure 5C). Western blot analysis of the 14 fractions showed that most endogenous and GFP-tagged EHD2 was present in a slowly sedimenting peak in fractions 2–4. Since this corresponded to an MW of 66–200 kDa (Hayer *et al*, 2010a), the peak probably contained the EHD2 dimers (MW of EHD2: 61 kDa). In addition, two peaks containing about 30% of total EHD2 were observed in fractions 9–12. This corresponded to complexes with sedimentation coefficients of 60 and 75S, which could mean that they have a molecular weight of about 2.5 and 3.5 MDa, respectively (Hayer *et al*, 2010a).

We have previously shown in similar gradients that CAV1 sediments as a large molecular weight complex of 70S (Hayer *et al*, 2010a). To determine whether EHD2 was part of the same complexes, we analysed cell lysates prepared using octylglucoside (OG), a non-ionic detergent that dissociates the CAV1 70S complex (Hayer *et al*, 2010a). As expected, CAV1 was now exclusively in fractions 3–4 corresponding to CAV1 8S complexes. However, EHD2 still sedimented as large oligomers indicating that EHD2 oligomers were distinct from the 70S CAV1 complex (Supplemenary Figure S5A). In addition, the EHD2 complexes were observed in MEF CAV1 −/− cells (Supplementary Figure S5B) showing that 60–75S EHD2 oligomers could form independently of caveolae.

Next, we tested the EHD2 mutants for their ability to form high MW complexes. HeLa cells transiently expressing tagged mutant proteins for 6–12 h were lysed and analysed on sucrose gradients. Mutations in the KPF/NPF motifs and deletion of the EH domain were found to most dramatically reduce oligomerization of EHD2 (Figure 5D; Supplementary Figure S5C), suggesting that the KPF/NPF motifs and EH domains were involved in 60–75S complex formation. This observation provided support for a model that involves the association of the EH domains of one dimer with KPF/NPF motifs of an adjacent dimer thus generating a linear or curved complex of EHD2 dimers as previously hypothesized (Daumke *et al*, 2007). A significant loss of high MW complexes was also detected for the lipid-binding mutant K327D, indicating that association with membranes and especially negatively charged phospholipids was required for oligomerization.

That the ATP-binding mutant (T72A) also was unable to form oligomers indicated a central function for the G domain (Figure 5D). Strikingly, the two other ATP-cycle mutants (EHD2-T94A and EHD2-I157Q) permitted formation of high MW complexes to the same extent as the wild-type protein (Figure 5D; Supplementary Figure S5C). This indicated that while ATP binding was necessary for oligomerization, ATP hydrolysis was not. Interestingly, the mutants that were unable to oligomerize all failed to associate with caveolae suggesting that not only was membrane binding required for oligomerization, but also oligomer formation was a prerequisite for caveolar association.

In combination with the localization data, our results suggested that the EHD2 present in the cytosol is in the dimeric form (Figure 1A). ATP binding allows the dimers to associate with lipids in the PM via the positively charged lipid-binding interface. Upon lipid binding, 60–75S EHD2 complexes are formed probably through interactions between the EH domains and the KPF/NPF sequence in an adjacent EHD2 dimer. As the ATP is hydrolysed, these complexes interact and accumulate at caveolae. Although caveolae are not needed for oligomerization, it is possible that oligomers in cells containing caveolae actually form in association with caveolae.

The ATPase domain regulates EHD2 dynamics and function

Further studies were performed with EHD2-I157Q–EGFP, which has an accelerated ATPase activity (Daumke *et al*, 2007), to elucidate the role of EHD2's G domain. The mutation in the P-loop of the G domain could either stabilize the catalytic conformation and prevent exchange of ADP to ATP (Li and Zhang, 2004), or impair the action of potential nucleotide exchange factors facilitating ADP to ATP exchange. FRAP experiments revealed that EHD2-I157Q–EGFP failed to recycle after association with caveolae (Figure 6A and B). This led us to express wild-type EHD2–mCherry and EHD2-I157Q–EGFP together. The EHD-I157Q–EGFP was now found trapped in caveolae with very little or no wild-type EHD2 present (Figure 6C). In contrast to wild-type EHD2, EHD2-I157Q was thus unable to dissociate resulting in the exclusion of wild-type EHD2. While ATP was needed to dissociate EHD2 from caveolae, too rapid hydrolysis evidently prevented displacement of EHD2 from caveolae. Consistent with a role for ATP in EHD2 dissociation from caveolae, we found that after depletion of cellular ATP with 2-deoxyglucose and sodium azide for 40 min, caveolae remained decorated with EHD2–GFP (Figure 6D).

Strikingly, when EHD2-I157Q was expressed in CAV1 −/− cells, it showed a punctate distribution (Figure 6E). This was in clear contrast to wild-type EHD2 that required the presence of caveolae to form similar puncta (Figure 1C). When CAV1 −/− cells were transfected with EHD2-I157Q and CAV1 together, the mutant EHD2 showed a punctate distribution that now perfectly overlapped with CAV1 signal (Supplementary Figure S5D). These experiments suggested that EHD2 puncta were assemblies of EHD2 complexes whose formation depended on ATP hydrolysis. In the case of wild-type EHD2, it seemed likely that association with caveolae stimulated ATP hydrolysis and resulted in EHD2 enrichment at caveolae. In contrast, the I157Q mutant with intrinsically accelerated ATP-hydrolysis rate could form EHD2 puncta independently of caveolae.

When EHD2-T72A–mCherry, the EHD2 mutant incapable of binding ATP was overexpressed in HeLa cells stably expressing CAV1–EGFP, we noticed that the amount of mobile caveolae was significantly enhanced (Figure 6F). The phenotype was comparable to the impact of EHD2 knockdown on CAV1 motility (Figure 2B). The result supported the conclusion that EHD2 is involved in promoting mechanisms that render caveolae in the PM stationary. To test whether the mutant had a dominant-negative effect, we co-expressed EHD2-T72A–mCherry and wild-type EHD2–EGFP in CV1 cells. Indeed, we found that wild-type EHD2 no longer localized to caveolae (Figure 6G) indicating that the presence of EHD2-T72A impaired wild-type EHD2 function. A possible explanation was that mixed or mutant EHD2 dimers could not form 60–75S complexes with mixed or mutant dimers, and were thus defective in PM association and oligomer formation.

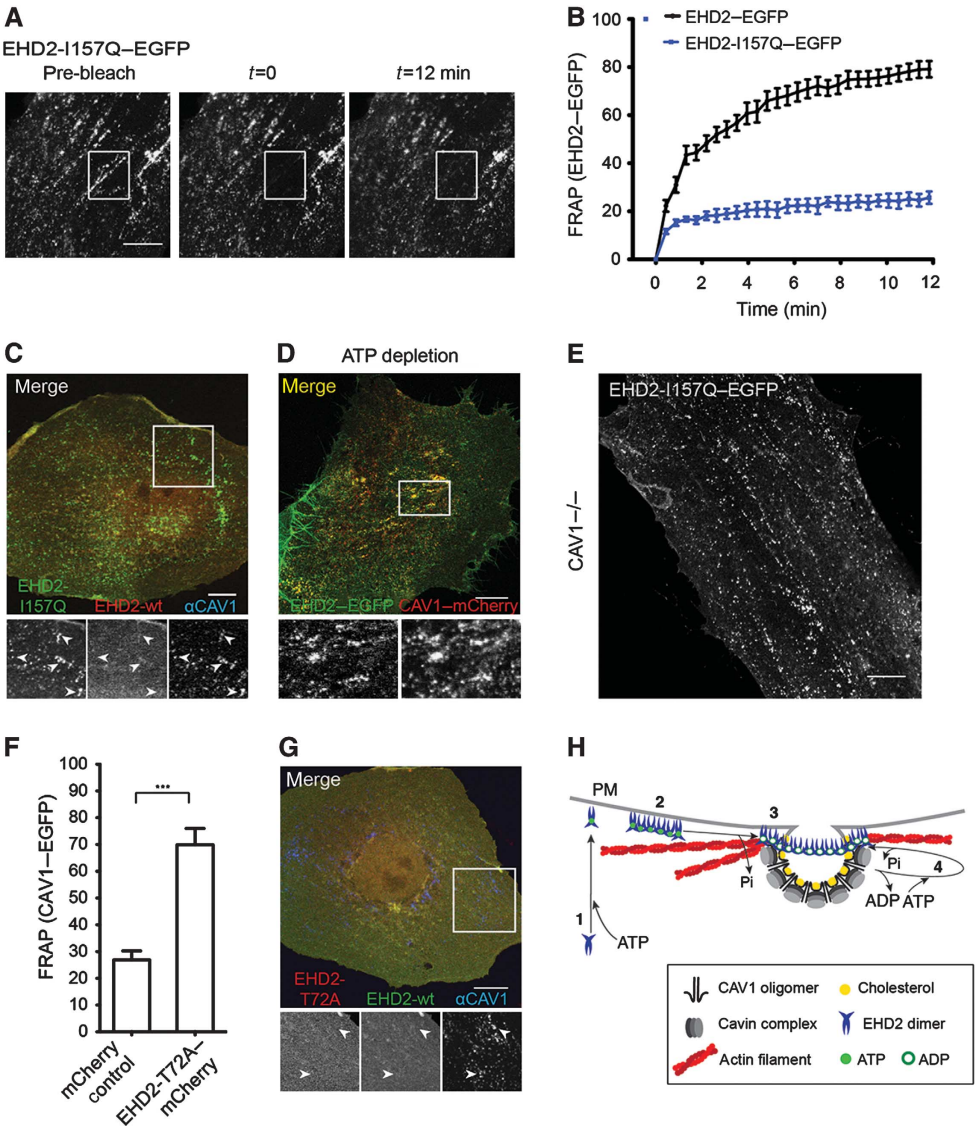

Figure 6 The ATPase domain regulates EHD2 dynamics and function. (**A**) Representative confocal images of FRAP experiments with EHD2-I157Q–EGFP expressing cells. No fluorescence recovery at initially bleached spots can be detected during the recorded time. (**B**) FRAP curves of EHD2–EGFP or EHD2-I157Q–EGFP-transfected CV1 cells (as in Figure 4D). Data points present mean values ± s.e.m., $n = 10$ or 8 for EHD2–EGFP or EHD2-I157Q–EGFP. (**C**) Representative confocal image of a CV1 cell co-expressing EHD2-I157Q–EGFP and EHD2–mCherry for 12 h. Cells were fixed and stained for endogenous CAV1. Arrows in the magnification highlight EHD2-I157Q-positive spots that have weak/no EHD2 wild-type staining and colocalize with CAV1. (**D**) CV1 cells transfected with EHD2–EGFP and CAV1–mCherry were incubated for 40 min in ATP-depletion media and analysed by confocal microscopy. Magnification highlights colocalization of EHD2 and CAV1. (**E**) Confocal image of MEF CAV1 $-/-$ cell transfected with EHD2-I157Q–EGFP for 6 h. (**F**) Relative CAV1 fluorescence 12 min after bleaching peripheral regions in HeLa cells, stably expressing CAV1–EGFP and transfected with mCherry control ($n = 11$) or EHD2-T72A–mCherry ($n = 11$) plasmids. Significance of mean differences between the conditions was calculated with a two-tailed unpaired *t*-test. ***P-value < 0.0001. (**G**) Representative confocal image of a CV1 cell co-expressing EHD2–EGFP and EHD2-T72A–mCherry. Cells were fixed and stained for endogenous CAV1. Arrows in the magnification highlight that CAV1-positive spots are devoid of wild-type EHD2 and EHD2-T72A. All scale bars 10 μm. (**H**) A model on the role of oligomer formation and the ATP cycle in EHD2 association with caveolae and dynamic exchange. (1) Newly synthesized EHD2 dimers bind ATP and are subsequently targeted to the plasma membrane via ionic interactions with negatively charged lipids. (2) Upon lipid binding, EHD2 dimers assemble into 60–75S oligomers via interactions of EH domain and KPF/NPF motifs in adjacent EHD2 dimers. (3) Association of EHD2 complexes with caveolae requires ATP hydrolysis, which may be stimulated at caveolae. (4) EHD2 proteins undergo dynamic exchange at caveolae, which requires a new cycle of ATP binding and hydrolysis. EHD2 mediates a link to actin fibres that run in close proximity to caveolae.

In summary, our data on the G-domain mutants showed that ATP binding was required for PM association of EHD2 and for the formation of 60–75S complexes. The ATP was hydrolysed when the 60–75S complexes associated with caveolae. That the EHD2-I157Q mutant protein with accelerated ATPase activity was unable to shuttle off caveolae was presumably because it could not hold ATP for long without hydrolysing it to ADP. Unlike wild-type EHD2, it was able to form assemblies of several 60–75S complexes in the absence of caveolae suggesting that it did not require caveolae to activate ATP hydrolysis. Moreover, EHD2-T72A, another mutant, acted as a dominant-negative mutant and caused increased caveolar motility.

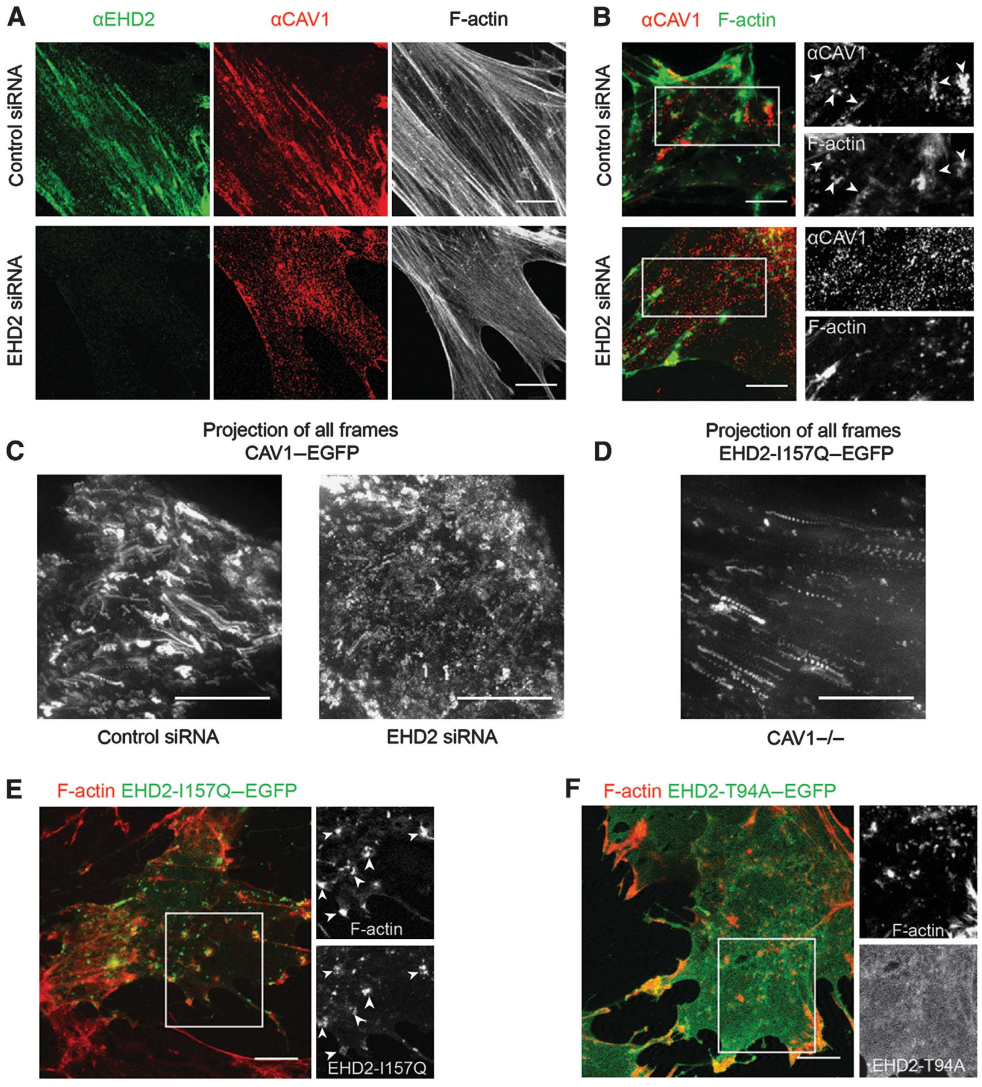

Figure 7 EHD2 oligomers mediate a link of caveolae to F-actin. (**A**) Confocal images of primary human fibroblasts immunostained with EHD2 and CAV1 antibodies and stained with fluorescent Phalloidin to visualize filamentous actin. Cells were transfected with control siRNA or EHD2 siRNA. (**B**) Confocal images of human fibroblasts transfected with control siRNA or EHD2 siRNA and treated for 5 min with 5 μM CytoD. CAV1 and Phalloidin signal is depicted. Side panels show enlargements of indicated regions in the merged images. Arrowheads highlight CAV1 close to actin patches. (**C**) HeLa cells stably expressing CAV1–EGFP were treated with control siRNA or EHD2 siRNA and transfected with RFP–actin (not depicted). Image depicts the CAV1–EGFP maximum intensity projection of all frames of a 7.5-min TIR-FM movie (90 frames, frame rate 0.2 Hz, penetration depth 110 nm) starting upon addition of 5 μM CytoD. Distinct trajectories of caveolae moving in the PM plane due to actin retraction can only be seen in control conditions. (**D**) CAV1 − / − cells were transfected with EHD2-I157Q–EGFP and RFP–actin (not depicted), treated with CytoD and live imaged as in **C**. (**D**) Maximum intensity projection of EHD2-I157Q–EGFP signal reveals retracting puncta. (**E**) Confocal images of CAV1 − / − cells, transfected with EHD2-I157Q–EGFP, treated for 5 min with 5 μM CytoD and stained with fluorescent Phalloidin. Side panels show enlargements of indicated region in the merged image. Arrowheads highlight EHD2 close to actin patches. (**F**) Confocal images of CAV1 − / − cells, transfected with EHD2-T94A–EGFP, treated and analysed as in **E**. All scale bars 10 μm.

EHD2 oligomers link caveolae to the actin cortex

In many cell types, caveolae tend to be aligned along actin filaments as shown for primary human fibroblasts immunostained for endogenous CAV1 and EHD2 (Figure 7A). When cytochalasin D (CytoD) was added to disrupt the actin filaments, the stress fibres rapidly disappeared and remaining F-actin accumulated in patches. The distribution of caveolae also changed; CAV1 now clustered around the F-actin aggregates (Figure 7B). TIR-FM time-lapse movies of HeLa cells expressing CAV1–EGFP and EHD2–mCherry allowed us to follow the impact of CytoD-induced actin filament disruption in live cells. They showed that after CytoD addition, the majority of CAV1 and EHD2-containing puncta moved along linear trajectories for distances of several microns, and came to rest in clusters (Supplementary Movie S5). Movies made of cells expressing RFP–actin and CAV1–EGFP confirmed that the caveolae were dragged along with the retracting actin in the plane of the PM and that the clusters colocalized with F-actin remnants (Figure 7C; Supplementary Movie S6). This indicated that the caveolae were tethered to filamentous actin.

The distribution and behaviour of caveolae was dramatically altered when EHD2 was depleted by siRNA. Instead of localizing in linear arrays along microfilaments, the CAV1-containing spots were now evenly distributed in human fibroblasts (Figure 7A). Addition of CytoD caused the

redistribution of actin in the same way as in control cells, but this failed to affect the distribution of CAV1. CAV1 continued to be localized in discrete puncta randomly distributed over the PM (Figure 7B). Consistently, actin filament disruption with CytoD had little effect on caveolar distribution in EHD2 siRNA-treated HeLa cells expressing RFP–actin and CAV1–EGFP imaged by TIR-FM (Figure 7C; Supplementary Movie S7). The movies showed that CAV1 spots remained motile as previously described (Figure 2). This indicated that the tethering of caveolae to microfilaments depended on EHD2.

To determine whether EHD2 was itself able to associate with F-actin and thus serve as a tether, we analysed MEF cells devoid of CAV1. Experiments documented in Figure 1C had already shown that when expressed in CAV1 −/− cells wild-type EHD2–EGFP did not form puncta nor did it align itself with stress fibres. However, it was also clear as shown in Figure 6 that when the EHD2 mutant with accelerated ATPase activity (EHD2-I157Q–EGFP) was expressed in the CAV1 −/− cells, the protein did form puncta and that the majority of these puncta aligned themselves into linear arrays (Figure 6E). After CytoD treatment, the linear arrays disappeared and the EHD2-I157Q spots retracted with F-actin and accumulated in actin patches similarly to those observed for CAV1 and wild-type EHD2 (Figure 7D and E; Supplementary Movie S8). In contrast another mutant, the PM-associated mutant EHD2-T94A–EGFP unable to hydrolyse ATP, showed a diffuse PM localization and was not affected by CytoD treatment (Figure 7F). Taken together, this showed that EHD2 complexes can link up with F-actin without being associated with caveolae. However, for this to happen, the ATPase activity has to be accelerated suggesting that the EHD2 needs to be in the ADP-bound form.

Discussion

Our results showed that EHD2 constitutes a major component of invaginated caveolae and caveolar clusters. It is recruited from the cytosol to the PM, and present as large 60–75S complexes, the formation of which requires ATP binding and membrane association. The EHD2 complexes are responsible for tethering caveolae to actin filaments and preventing their lateral movement and the formation of caveolar vesicles. Unlike CAV1 and the cavins, which are stable components of caveolae, EHD2 undergoes a continuous turnover driven by the binding and hydrolysis of ATP.

The majority of caveolae in the PM are static (Thomsen *et al*, 2002; van Deurs *et al*, 2003; Kirkham *et al*, 2005; Pelkmans and Zerial, 2005; Tagawa *et al*, 2005). Integrin expression, insulin activation, and the addition of phosphatase inhibitors, gangliosides or SV40 are known to activate caveolae and induce the generation of mobile, endocytic caveolar vesicles (Parton *et al*, 1994; Pelkmans *et al*, 2002; Kirkham and Parton, 2005; Sharma *et al*, 2005; Parton and Simons, 2007; Botos *et al*, 2008; Lajoie and Nabi, 2010; Singh *et al*, 2010). We found that depletion of EHD2 by RNAi and expression of a dominant-negative EHD2 mutant significantly elevated the fraction of mobile caveolae without external stimuli. Since the caveolar vesicles formed contained cavin-1 and their formation was dependent on dynamin, they were likely to be derived from the PM.

Consistent with a constraining role, we found that when EHD2 was overexpressed the endocytic function of caveolae was suppressed. We followed CT-B a ligand known to be internalized via caveolae when added at low concentrations (Parton, 1994; Pelkmans *et al*, 2004). It accumulated in EHD2-positive caveolae in the PM, and delivery to the Golgi complex was decreased. A similar reduction in Golgi-localized CT-B signal after overexpressing EHD2 was recently reported by Benjamin *et al* (2011).

In cells, EHD2 occurred in different oligomeric forms. The majority was present in a slowly sedimenting form that most likely corresponded to soluble homo-dimers (Figure 1A; Daumke *et al*, 2007). This was the only form observed when lipid or ATP binding was compromised through point mutations in the respective domains. About 30% of EHD2 sedimented as complexes of 60 and 75S with estimated molecular weights in the 2.5–3.5 MDa range. Since efficient formation of these large complexes required a functional lipid-binding domain, they were probably membrane associated. Experiments with mutants indicated furthermore that the formation of these complexes required, in addition to lipid and ATP, a functional EH domain, and intact KPF/NPF motifs to which EH domains specifically bind.

In-vitro experiments by Daumke *et al* (2007) have shown that in the presence of ATP and liposomes containing acidic phospholipids, isolated EHD2 oligomerizes to form circular, liposome-associated assemblies with about 20 dimers. These have a calculated molecular weight similarly to the estimated weight of the complexes that we observed in cell extracts. Daumke *et al* (2007) hypothesized that the EH domains of one dimer interact with the KPF/NPF motifs of neighbouring dimers resulting in the generation of a linear complex. Given the similarities in size and assembly requirements, it is likely that the 60 and/or 75S complexes observed in cells are equivalent to the complexes observed *in vitro*. In other words, the 60 and 75S complexes may represent linear or circular assemblies of EHD2 attached to the head groups of negatively charged lipids such as phosphatidylserine in the inner leaflet of the PM.

The architecture of caveolar domains is remarkably in that the major protein components all exist as large, oligomeric complexes. We have shown previously that CAV1 and the cavins are present as independent assemblies with sedimentation coefficients in the 60–70S range (Hayer *et al*, 2010a). Like the EHD2, the cavins are peripheral membrane proteins recruited from the cytosol (Bastiani *et al*, 2009; Hayer *et al*, 2010a). Both EHD2 and the cavins have affinity for negatively charged phospholipids and the formation of complexes is independent of CAV1 (Blume *et al*, 2007; Daumke *et al*, 2007; Hill *et al*, 2008; Bastiani *et al*, 2009; Hayer *et al*, 2010a). Their affinity for caveolar domains may be explained by the postulated enrichment of phospatidylserine induced by CAV1 (Pike *et al*, 2002; Wanaski *et al*, 2003).

Using mutants of EHD2, we found that the formation of the 60–75S complexes was not sufficient for association with caveolae. The ATPase activity was also needed. It remains to be determined whether the hydrolysis of ATP is required to induce interactions between 60 and 75S complexes or to promote association with other structures in caveolar domains. However, it was apparent that multiple 60–75S complexes were recruited to each caveolae because only after caveolar association was fluorescent EHD2 detectable as defined spots. It is interesting in this context that the I157Q mutant of EHD2 with accelerated ATPase activity was able to

form spots of similar dimensions and fluorescence intensity and to associate with actin filaments in the absence of caveolae. This could imply that association with the caveolar domain somehow increases the ATPase activity of wild-type EHD2 complexes and promotes mulitmerization and actin binding. *In-vitro* experiments have shown that the ATPase activity can be accelerated by addition of negatively charged lipids (Daumke *et al*, 2007).

The existence of an interaction between the actin cytoskeleton and caveolae has been proposed in several morphological studies. These show microfilaments in close proximity to caveolae, and one of the studies identifies crossbridges between caveolae and actin fibres (Rothberg *et al*, 1992; Richter *et al*, 2008). The actin cytoskeleton is also known to affect caveolae at the functional level. On the one hand, it is thought that it controls internalization by confining caveolae to the PM. On the other hand, actin is thought to promote efficient caveolar internalization after stimulation (Parton *et al*, 1994; Stahlhut and van Deurs, 2000; Mundy *et al*, 2002; Pelkmans *et al*, 2002; Sverdlov *et al*, 2009).

Our results were consistent with the existence of an intimate connection between stationary caveolae and the actin cytoskeleton. Using CytoD to collapse the microfilament network, we could show in live cells that the EHD2-containing caveolae moved together with the collapsing fibres. EHD2 depletion resulted in a loss of this connection; most of the caveolae now showed increased motility and failed to be dragged along by the collapsing microfilaments. EHD2 was probably itself part of the structure that formed the physical link between caveolae and actin filaments. This was suggested by an EHD2 mutant that possessed an elevated ATP hydrolysis rate. Unlike wild-type EHD2, it formed actin-associated puncta even in the absence of caveolae. The attachment of EHD2 with caveolae was not permanent as observed for CAV1 and the cavins. FRAP experiments showed that the EHD2 was dynamically associated with caveolae and underwent turnover. The half-life was about 2–4 min, and the presence of ATP was required. Although relatively slow, this turnover is probably significant because it may allow adjustment and fine-tuning of caveolar dynamics.

Taken together, our results demonstrated that EHD2 is a critical factor in regulating the dynamic behaviour of caveolae and defining their role in clathrin-independent endocytosis. A concomitant study confirms the importance of EHD2 in constraining caveolae to the PM (Moren *et al*, 2012). The authors find that EHD2 specifically associates with caveolae at the cell surface. Upon EHD2 depletion, they detect an increased amount of dynamin-dependent caveolar budding. We further showed that when EHD2 complexes associate with caveolae in the PM, they decrease caveolar motility, increase clustering, and suppress formation of caveolar vesicles by mediating an immobilizing link to the actin cortex. This confinement regimen can evidently be reversed by external stimuli that allow endocytosis to occur. It is likely that in promoting the link, EHD2 interacts with other cellular proteins. Possible interaction partners are EHBP1 shown to bind EHD2 and colocalize with F-actin (Guilherme *et al*, 2004), the actin crosslinking protein filamin A described as a linker between caveolae and actin in caveolar anchorage and internalization (Sverdlov *et al*, 2009; Muriel *et al*, 2011), and other cytoskeletal proteins identified at the neck of caveolae (Foti *et al*, 2007). It is possible that EHD2 has other functions such as preventing the action of the membrane scission factor dynamin-2 (Jakobsson *et al*, 2011). While EHD2 seems to be specifically responsible for caveolar confinement, it remains unclear which factors regulate the release of EHD2 proteins from caveolae to allow caveolar scission and internalization.

Materials and methods

Cell culture and transfections

CV1 (ATCC), HeLa (ATCC), normal human primary dermal fibroblasts (ATCC), and CAV1−/− MEFs (Drab *et al*, 2001) were grown in DMEM (Invitrogen), supplemented with 10% FCS and 1% glutamax (Invitrogen). HeLa-CAV1–EGFP or HeLa-cavin-1–EGFP were grown as HeLa, but in the presence of 0.5 mg/ml G418 or 0.5 μg/ml puromycin. 3T3-L1 pre-adipocytes (ATCC) were grown in DMEM (Invitrogen), supplemented with 10% bovine serum and 1% glutamax (Invitrogen). CV1, HeLa, and CAV1 −/− cells were transfected by electroporation (AMAXA) or using Lipofectamine 2000 (Invitrogen) according to manufacturer's recommendations.

Plasmids

For EHD2–mEGFP and EHD2–mCherry, human EHD2 cDNA from an ORFeome collection (V3.1 Open Biosystems) was cloned into pmEGFP-N-DEST or pmCherry-N-DEST destination vectors carrying a Gateway cassette. QuikChange site directed mutagenesis (Stratagene) was used to obtain point mutants (T72A, T94A, I159Q, and K327D). The KPF/NPF (F122A/F128A) mutant was generated by sequential mutagenesis. The EHD2–mCherry rescue plasmid was generated by silently mutating two nucleotides in the region targeted by EHD2 siRNA SI04205271 with QuikChange PCR. EHD2-ΔEH was acquired by PCR of EHD2 amino acids 1–448. Dynamin2-K44A-mRFP (splice variant IIA) was derived from Dyn2-K44A-GFP generously provided by Mark A McNiven by exchanging GFP with mRFP. Cavin-3–EGFP was generated by PCR amplifying human cavin-3 and cloning into a pIRESpuro-EGFP vector. EHD1, EHD3, and EHD4 were a kind gift of Manju George (George *et al*, 2007). Other constructs have previously been described: CAV1–mEGFP, CAV1–mCherry, CAV1–HA, Flot1–EGFP, Flot2-EGFP, cavin-1–mEGFP, cavin-1–mCherry, cavin-2–EGFP (Hayer *et al*, 2010a), Rab5–EGFP (Hayer *et al*, 2010b), and CLC-GFP (Tagawa *et al*, 2005).

RNAi

The siRNA oligomers targeting EHD2 (SI04205271 and SI04315108) were purchased from QIAGEN and transfected into HeLa, human fibroblast, HeLa-CAV1–EGFP, or HeLa-cavin-1–EGFP at 15 nM using Lipofectamine RNAiMAX (Invitrogen) according to manufacturer's recommendations. Non-targeting siRNA (AllStarsNeg; QIAGEN) was used as control siRNA. Cells were analysed 60–72 h after transfection.

Antibodies and other reagents

Rabbit pAb anti-CAV1 was from Santa Cruz (N20, sc-894), rabbit pAb anti-cavin-1 from Abcam (ab48824), mouse mAb anti-GFP from Living Colours (JL-8), rabbit pAb anti-EHD2 from Santa Cruz (sc-100724, used for WB), goat pAb anti-EHD2 from Abcam (ab23935, used for IF), rabbit pAb anti-giantin from Covance (PRB-114C), and mAb anti-β-actin (A1978) was from Sigma. Alexa Fluor-conjugated secondary antibodies for immunofluorescence were from Invitrogen.

For disruption of F-actin, cells were incubated with 5 μM Cytochalasin D. For ATP depletion, cells were washed and incubated in glucose-free media with 10 mM 2-deoxy-D-glucose and 10 mM sodium azide. All chemicals were purchased from Sigma-Aldrich.

Immunofluorescence imaging and analysis

Cells grown on coverslips were fixed using 4% formaldehyde in PBS. Cells were permeabilized using 0.05% saponin and 1% BSA in PBS and incubated with the appropriate primary (1:500) and secondary (1:1000) antibodies, and coverslips were mounted on slides using Immu-Mount (Thermo Scientific). Imaging was performed on an inverted confocal microscope system (LSM 510 Meta; Carl Zeiss, Inc.). Colocalization of CAV1 spots with proteins of

interest was quantified in ImageJ. A thresholding was applied to the CAV1 channel. Coordinates of caveolar spots were extracted with the 'analyse particles' function and checked for colocalization with protein of interest.

Fluorescence recovery after photobleaching

For FRAP experiments that quantified caveolar movement, either HeLa-CAV1–mEGFP cells or HeLa-cavin-1–EGFP cells were treated with siRNA for 60–72 h. On the day prior to acquisition, cells were plated on 18 mm coverslips. For FRAP experiments that quantified recovery of cavins or EHD2 at stationary caveolae, EGFP-tagged cavins or EHD2 together with CAV1–mCherry were expressed in CV1 cells for 14 h. FRAP experiments were performed at 37°C on an inverted confocal microscope system (LSM 510 Meta) equipped with a temperature-controlled stage and a $\times 100$ 1.4 NA objective with $2\times$ zoom as described previously (Tagawa *et al*, 2005). A defined region was bleached at 100% laser transmission for 25 iterations using the 488-nm line from a 30-mW Argon laser and fluorescence recovery was monitored by scanning a defined region at low laser transmission (50% power, 3% transmission) every 20 s for 30 frames. Images were acquired as 12-bit LSM files at 512×512 pixels/frame and 0.14 μm/pixel lateral resolution. Image series with little or no apparent motion of cells were quantified with ImageJ. The mean fluorescence intensity of the bleached region at each time point was corrected for background signal and photobleaching of the cell as in Tagawa *et al* (2005). Fluorescence intensity before bleaching was normalized to 100% and directly after bleaching to 0%. For FRAP experiments of cavins and EHD2 at stationary caveolae, an image of CAV1–mCherry was recorded before and after the image series to assure that anchored caveolae had not moved in the recorded time.

Fluorescence resonance energy transfer

FRET efficiency was determined by performing acceptor photobleaching with subsequent measurement of donor dequenching with the fluorophore pairs EGFP (donor) and mCherry (acceptor). Cells in 8-well Labtek chambers (Thermo Scientific) were transiently transfected (Lipofectamine 2000) with fluorescent fusion proteins and expression allowed for 14 h. Cells were fixed with 4% methanol-free formaldehyde (Thermo Scientific) and subsequently imaged in PBS. FRET analysis was performed using a Leica SP2-FCS microscope. EGFP was excited with 20% 488 nm laser intensity and emission was detected at 505–550 nm. mCherry was excited with 20% 561 nm laser intensity and emission detected at 610–685 nm. Images were taken with $\times 63$ 1.4 NA DIC, Oil, HCX Plan-Apo objective, $3\times$ zoom and a pinhole of one airy unit with focus on the PM. Bleaching was performed with 100% 561 nm intensity and 20 iterations. Images were analysed using the Leica LCS Imaging software. To determine FRET efficiency, donor fluorescence intensity before (D_{pre}) and after (D_{post}) photobleaching was measured in membrane spots (= region of interest (ROI)) within the bleached and non-bleached region for each cell and the background subtracted. FRET efficiency was calculated for every ROI of the imaged cell according to the formula: $(D_{post} - D_{pre})/D_{post} \times 100$. For statistical analysis, the mean FRET efficiency in ROIs within bleached and non-bleached regions was determined for every cell and significance between means analysed with a two-tailed paired *t*-test.

CT-B uptake

CV1 cells were transfected with EHD2–mCherry using AMAXA, seeded onto glass coverslips and expression allowed for 14 h. Cells were incubated at 37°C with 50 ng/ml Alexa Fluor 488-labelled CT-B (Molecular Probes). After 30 min, cells were washed $3\times$ followed by a 30-min chase at 37°C, washed and fixed for 20 min in 4% FA in PBS. Subsequently, cells were stained for Giantin or CAV1 and imaged with confocal microscopy. For quantification of CT-B signal in the Golgi region, a custom-made ImageJ based software was used to define the Golgi region, to measure the mean intensity of CT-B-488 signal in these areas and to subsequently score cells for being EHD2-mCherry positive or negative in each image. Localization of CT-B in caveolar spots after the 30-min chase was analysed with ImageJ using thresholding and particle analysis to obtain coordinates of CAV1 or CAV1 + EHD2-mCherry-positive puncta that were subsequently checked for colocalization with CT-B-488.

Live-cell fluorescence imaging

CV1 cells expressing fluorescently tagged constructs and seeded onto 18 mm coverslips were transferred to a custom-built metal microscope coverslip chamber in CO_2-independent medium (Invitrogen), supplemented with 10% FCS. A Leica AM TIRF system was used, equipped with a $\times 100$ 1.47 NA objective, an Andor iXon EM-CCD camera and a temperature-controlled stage. The depth of the evanescent field was adjusted to the indicated penetration depth. EGFP and mCherry channels were acquired sequentially. Image sequences were analysed by ImageJ.

Immuno-EM

EHD2–EGFP and CAV1–HA were expressed in CV1 cells for 6 h. Cells were fixed in 4% formaldehyde and 0.1% glutaraldehyde in $1\times$ PHEM buffer for 90 min (Schliwa *et al*, 1981). Cryo-sectioning and immunolabelling were performed as described elsewhere (Tokuyasu, 1973). In brief, ultrathin sections (50–70 nm) from gelatin-embedded and frozen cell pellets were obtained using an FC7/UC7-ultramicrotome (Leica, Vienna, Austria). Immunogold labelling was carried out on thawed sections with anti-GFP (Rockland, 600-101-215) and anti-HA (Covance, HA-11) antibodies and 10 or 5 nm protein A-gold (UMC Utrecht University, Utrecht, Netherlands) (1:50). Sections were examined with a CM10 Philips transmission electron microscope with an Olympus 'Veleta' 2kx2k side-mounted TEM CCD camera. For colocalization analysis, the cryo-sections were followed in a meandering pattern. Screening along the PM, visible colocalization events of 5 and 10 nm gold particles were counted and scored as caveolae or non-caveolae structure based on invaginated morphology in four independent scans, each counting >200 gold particles. To determine the distance of EHD2 and CAV1 gold particles from the PM, perpendicular measurements towards the PM were performed from 10 or 5 nm gold particles within a maximal distance of 300 nm from the membrane.

Velocity gradient centrifugation

Sucrose velocity gradient centrifugation was performed as described previously (Hayer *et al*, 2010a). Cells were lysed for 20 min at room temperature in 0.5% Triton X-100 (TX100) or (if specifically indicated) in 60 mM OG in TNE (20 mM Tris–HCl, HpH 7.4, 100 mM NaCl, and 5 mM EDTA) supplemented with Complete protease inhibitor cocktail (Roche). Postnuclear supernatants were loaded onto 10–40% linear sucrose gradients prepared in 0.15% TX100/TNE or 35 mM OG/TNE and spun in a rotor (SW55Ti; Beckman Coulter) at 50 000 r.p.m. (237 020 *g*) at 4°C for 255 min. Gradient fractions were analysed by SDS–PAGE/western blotting.

Supplementary data

Supplementary data are available at *The EMBO Journal* Online (http://www.embojournal.org).

Acknowledgements

We are grateful to Arnold Hayer for experimental advice throughout the project and critical reading of the manuscript. We thank Nikolaus Schmitz for help with the PyMOL software, Manju George for EHD1-4 constructs, the Light Microscopy Centre of ETH Zurich and members of the Helenius laboratory for support, especially Florian Schmidt and Jason Mercer for comments on the manuscript. We thank Prof. H Stahlberg for supporting CB with working space and EM equipment. Funding was provided by ETH Zurich, the European Research Council (ERC), and the SNF Sinergia Projects. MS was supported by a Boehringer Ingelheim Fonds PhD fellowship.

Author contributions: MS, IKS, CH, and CKB performed the experiments; MS, IKS, CH, CKB, and GB analysed the data; MS and AH conceived and designed the experiments, MS and AH wrote the manuscript.

Conflict of interest

The authors declare that they have no conflict of interest.

References

Aboulaich N, Vainonen JP, Stralfors P, Vener AV (2004) Vectorial proteomics reveal targeting, phosphorylation and specific fragmentation of polymerase I and transcript release factor (PTRF) at the surface of caveolae in human adipocytes. *Biochem J* **383:** 237–248

Bastiani M, Liu L, Hill MM, Jedrychowski MP, Nixon SJ, Lo HP, Abankwa D, Luetterforst R, Fernandez-Rojo M, Breen MR, Schedl A, Haller H, Kurzchalia TV (2009) MURC/Cavin-4 and cavin family members form tissue-specific caveolar complexes. *J Cell Biol* **185:** 1259–1273

Benjamin S, Weidberg H, Rapaport D, Pekar O, Nudelman M, Segal D, Hirschberg K, Katzav S, Ehrlich M, Horowitz M (2011) EHD2 mediates trafficking from the plasma membrane by modulating Rac1 activity. *Biochem J* **439:** 433–442

Blume JJ, Halbach A, Behrendt D, Paulsson M, Plomann M (2007) EHD proteins are associated with tubular and vesicular compartments and interact with specific phospholipids. *Exp Cell Res* **313:** 219–231

Botos E, Klumperman J, Oorschot V, Igyarto B, Magyar A, Olah M, Kiss AL (2008) Caveolin-1 is transported to multi-vesicular bodies after albumin-induced endocytosis of caveolae in HepG2 cells. *J Cell Mol Med* **12:** 1632–1639

Boucrot E, Howes MT, Kirchhausen T, Parton RG (2011) Redistribution of caveolae during mitosis. *J Cell Sci* **124:** 1965–1972

Chinnapen DJ, Chinnapen H, Saslowsky D, Lencer WI (2007) Rafting with cholera toxin: endocytosis and trafficking from plasma membrane to ER. *FEMS Microbiol Lett* **266:** 129–137

Daumke O, Lundmark R, Vallis Y, Martens S, Butler PJ, McMahon HT (2007) Architectural and mechanistic insights into an EHD ATPase involved in membrane remodelling. *Nature* **449:** 923–927

Drab M, Verkade P, Elger M, Kasper M, Lohn M, Lauterbach B, Menne J, Lindschau C, Mende F, Luft FC, Schedl A, Haller H, Kurzchalia TV (2001) Loss of caveolae, vascular dysfunction, and pulmonary defects in caveolin-1 gene-disrupted mice. *Science* **293:** 2449–2452

Foti M, Porcheron G, Fournier M, Maeder C, Carpentier JL (2007) The neck of caveolae is a distinct plasma membrane subdomain that concentrates insulin receptors in 3T3-L1 adipocytes. *Proc Natl Acad Sci USA* **104:** 1242–1247

Fra AM, Williamson E, Simons K, Parton RG (1995) *De novo* formation of caveolae in lymphocytes by expression of VIP21-caveolin. *Proc Natl Acad Sci USA* **92:** 8655–8659

George M, Ying G, Rainey MA, Solomon A, Parikh PT, Gao Q, Band V, Band H (2007) Shared as well as distinct roles of EHD proteins revealed by biochemical and functional comparisons in mammalian cells and C. elegans. *BMC Cell Biol* **8:** 3

Guilherme A, Soriano NA, Bose S, Holik J, Bose A, Pomerleau DP, Furcinitti P, Leszyk J, Corvera S, Czech MP (2004) EHD2 and the novel EH domain binding protein EHBP1 couple endocytosis to the actin cytoskeleton. *J Biol Chem* **279:** 10593–10605

Hansen CG, Bright NA, Howard G, Nichols BJ (2009) SDPR induces membrane curvature and functions in the formation of caveolae. *Nat Cell Biol* **11:** 807–814

Hansen CG, Howard G, Nichols BJ (2011) Pacsin 2 is recruited to caveolae and functions in caveolar biogenesis. *J Cell Sci* **124:** 2777–2785

Hansen CG, Nichols BJ (2010) Exploring the caves: cavins, caveolins and caveolae. *Trends Cell Biol* **20:** 177–186

Hayer A, Stoeber M, Bissig C, Helenius A (2010a) Biogenesis of caveolae: stepwise assembly of large caveolin and cavin complexes. *Traffic* **11:** 361–382

Hayer A, Stoeber M, Ritz D, Engel S, Meyer HH, Helenius A (2010b) Caveolin-1 is ubiquitinated and targeted to intralumenal vesicles in endolysosomes for degradation. *J Cell Biol* **191:** 615–629

Henley JR, Krueger EW, Oswald BJ, McNiven MA (1998) Dynamin-mediated internalization of caveolae. *J Cell Biol* **141:** 85–99

Hill MM, Bastiani M, Luetterforst R, Kirkham M, Kirkham A, Nixon SJ, Walser P, Abankwa D, Oorschot VM, Martin S, Hancock JF, Parton RG (2008) PTRF-Cavin, a conserved cytoplasmic protein required for caveola formation and function. *Cell* **132:** 113–124

Jakobsson J, Ackermann F, Andersson F, Larhammar D, Low P, Brodin L (2011) Regulation of synaptic vesicle budding and dynamin function by an EHD ATPase. *J Neurosci* **31:** 13972–13980

Kirkham M, Fujita A, Chadda R, Nixon SJ, Kurzchalia TV, Sharma DK, Pagano RE, Hancock JF, Mayor S, Parton RG (2005) Ultrastructural identification of uncoated caveolin-independent early endocytic vehicles. *J Cell Biol* **168:** 465–476

Kirkham M, Parton RG (2005) Clathrin-independent endocytosis: new insights into caveolae and non-caveolar lipid raft carriers. *Biochim Biophys Acta* **1745:** 273–286

Lajoie P, Nabi IR (2010) Lipid rafts, caveolae, and their endocytosis. *Int Rev Cell Mol Biol* **282:** 135–163

Lee DW, Zhao X, Scarselletta S, Schweinsberg PJ, Eisenberg E, Grant BD, Greene LE (2005) ATP binding regulates oligomerization and endosome association of RME-1 family proteins. *J Biol Chem* **280:** 17213–17220

Li G, Zhang XC (2004) GTP hydrolysis mechanism of Ras-like GTPases. *J Mol Biol* **340:** 921–932

McMahon KA, Zajicek H, Li WP, Peyton MJ, Minna JD, Hernandez VJ, Luby-Phelps K, Anderson RG (2009) SRBC/cavin-3 is a caveolin adapter protein that regulates caveolae function. *EMBO J* **28:** 1001–1015

Moren B, Shah C, Howes MT, Schieber NL, McMahon HT, Parton RG, Daumke O, Lundmark R (2012) EHD2 regulates caveola dynamics via ATP-driven targeting and oligomerization. *Mol Biol Cell* **23:** 1316–1329

Mundy DI, Machleidt T, Ying YS, Anderson RG, Bloom GS (2002) Dual control of caveolar membrane traffic by microtubules and the actin cytoskeleton. *J Cell Sci* **115:** 4327–4339

Muriel O, Echarri A, Hellriegel C, Pavon DM, Beccari L, Del Pozo MA (2011) Phosphorylated filamin A regulates actin-linked caveolae dynamics. *J Cell Sci* **124:** 2763–2776

Naslavsky N, Caplan S (2011) EHD proteins: key conductors of endocytic transport. *Trends Cell Biol* **21:** 122–131

Oh P, McIntosh DP, Schnitzer JE (1998) Dynamin at the neck of caveolae mediates their budding to form transport vesicles by GTP-driven fission from the plasma membrane of endothelium. *J Cell Biol* **141:** 101–114

Parton RG (1994) Ultrastructural localization of gangliosides; GM1 is concentrated in caveolae. *J Histochem Cytochem* **42:** 155–166

Parton RG, Joggerst B, Simons K (1994) Regulated internalization of caveolae. *J Cell Biol* **127:** 1199–1215

Parton RG, Simons K (2007) The multiple faces of caveolae. *Nat Rev Mol Cell Biol* **8:** 185–194

Pelkmans L, Burli T, Zerial M, Helenius A (2004) Caveolin-stabilized membrane domains as multifunctional transport and sorting devices in endocytic membrane traffic. *Cell* **118:** 767–780

Pelkmans L, Fava E, Grabner H, Hannus M, Habermann B, Krausz E, Zerial M (2005) Genome-wide analysis of human kinases in clathrin- and caveolae/raft-mediated endocytosis. *Nature* **436:** 78–86

Pelkmans L, Helenius A (2002) Endocytosis via caveolae. *Traffic* **3:** 311–320

Pelkmans L, Puntener D, Helenius A (2002) Local actin polymerization and dynamin recruitment in SV40-induced internalization of caveolae. *Science* **296:** 535–539

Pelkmans L, Zerial M (2005) Kinase-regulated quantal assemblies and kiss-and-run recycling of caveolae. *Nature* **436:** 128–133

Pike LJ, Han X, Chung KN, Gross RW (2002) Lipid rafts are enriched in arachidonic acid and plasmenylethanolamine and their composition is independent of caveolin-1 expression: a quantitative electrospray ionization/mass spectrometric analysis. *Biochemistry* **41:** 2075–2088

Richter T, Floetenmeyer M, Ferguson C, Galea J, Goh J, Lindsay MR, Morgan GP, Marsh BJ, Parton RG (2008) High-resolution 3D quantitative analysis of caveolar ultrastructure and caveola-cytoskeleton interactions. *Traffic* **9:** 893–909

Rothberg KG, Heuser JE, Donzell WC, Ying YS, Glenney JR, Anderson RG (1992) Caveolin, a protein component of caveolae membrane coats. *Cell* **68:** 673–682

Sargiacomo M, Scherer PE, Tang Z, Kubler E, Song KS, Sanders MC, Lisanti MP (1995) Oligomeric structure of caveolin: implications for caveolae membrane organization. *Proc Natl Acad Sci USA* **92:** 9407–9411

Schliwa M, Euteneuer U, Bulinski JC, Izant JG (1981) Calcium lability of cytoplasmic microtubules and its modulation by microtubule-associated proteins. *Proc Natl Acad Sci USA* **78:** 1037–1041

Sharma DK, Brown JC, Cheng Z, Holicky EL, Marks DL, Pagano RE (2005) The glycosphingolipid, lactosylceramide, regulates beta1-integrin clustering and endocytosis. *Cancer Res* **65:** 8233–8241

Sharma M, Naslavsky N, Caplan S (2008) A role for EHD4 in the regulation of early endosomal transport. *Traffic* **9:** 995–1018

Singh RD, Marks DL, Holicky EL, Wheatley CL, Kaptzan T, Sato SB, Kobayashi T, Ling K, Pagano RE (2010) Gangliosides and beta1-integrin are required for caveolae and membrane domains. *Traffic* **11:** 348–360

Sinha B, Koster D, Ruez R, Gonnord P, Bastiani M, Abankwa D, Stan RV, Butler-Browne G, Vedie B, Johannes L, Morone N, Parton RG, Raposo G, Sens P, Lamaze C, Nassoy P (2011) Cells respond to mechanical stress by rapid disassembly of caveolae. *Cell* **144:** 402–413

Stahlhut M, van Deurs B (2000) Identification of filamin as a novel ligand for caveolin-1: evidence for the organization of caveolin-1-associated membrane domains by the actin cytoskeleton. *Mol Biol Cell* **11:** 325–337

Sverdlov M, Shajahan AN, Minshall RD (2007) Tyrosine phosphorylation-dependence of caveolae-mediated endocytosis. *J Cell Mol Med* **11:** 1239–1250

Sverdlov M, Shinin V, Place AT, Castellon M, Minshall RD (2009) Filamin A regulates caveolae internalization and trafficking in endothelial cells. *Mol Biol Cell* **20:** 4531–4540

Tagawa A, Mezzacasa A, Hayer A, Longatti A, Pelkmans L, Helenius A (2005) Assembly and trafficking of caveolar domains in the cell: caveolae as stable, cargo-triggered, vesicular transporters. *J Cell Biol* **170:** 769–779

Thomsen P, Roepstorff K, Stahlhut M, van Deurs B (2002) Caveolae are highly immobile plasma membrane microdomains, which are not involved in constitutive endocytic trafficking. *Mol Biol Cell* **13:** 238–250

Tokuyasu KT (1973) A technique for ultracryotomy of cell suspensions and tissues. *J Cell Biol* **57:** 551–565

van Deurs B, Roepstorff K, Hommelgaard AM, Sandvig K (2003) Caveolae: anchored, multifunctional platforms in the lipid ocean. *Trends Cell Biol* **13:** 92–100

Wanaski SP, Ng BK, Glaser M (2003) Caveolin scaffolding region and the membrane binding region of SRC form lateral membrane domains. *Biochemistry* **42:** 42–56

